Research Article | Vol. 7, No. 11 | 1 Nov 2016 | BIOMEDICAL OPTICS EXPRESS 4441

Biomedical Optics EXPRESS

Combined frequency domain photoacoustic and ultrasound imaging for intravascular applications

ROBIN F. CASTELINO,[1,2,*] MICHAEL HYNES,[2] CHELSEA E. MUNDING,[1,2] SERGEY TELENKOV,[3] AND F. STUART FOSTER[1,2]

[1]*Medical Biophysics, University of Toronto, 5 King's College Road, Toronto, ON M5S 3G8, Canada*
[2]*Imaging Research, Sunnybrook Research Institute, 2075 Bayview Avenue, Toronto, Ontario M4N 3M5, Canada*
[3]*PHAST Imaging, 1B Richview Road, Toronto, ON M9A 4M6, Canada*
[*]*robin.castelino@utoronto.ca*

Abstract: Intravascular photoacoustic (IVPA) imaging has the potential to characterize lipid-rich structures based on the optical absorption contrast of tissues. In this study, we explore frequency domain photoacoustics (FDPA) for intravascular applications. The system employed an intensity-modulated continuous wave (CW) laser diode, delivering 1W over an intensity modulated chirp frequency of 4-12MHz. We demonstrated the feasibility of this approach on an agar vessel phantom with graphite and lipid targets, imaged using a planar acoustic transducer co-aligned with an optical fibre, allowing for the co-registration of IVUS and FDPA images. A frequency domain correlation method was used for signal processing and image reconstruction. The graphite and lipid targets show an increase in FDPA signal as compared to the background of 21dB and 16dB, respectively. Use of compact CW laser diodes may provide a valuable alternative for the development of photoacoustic intravascular devices instead of pulsed laser systems.

OCIS codes: (170.5120) Photoacoustic imaging; (170.7170) Ultrasound.

References and links

1. C. V. Bourantas, H. M. Garcia-Garcia, K. K. Naka, A. Sakellarios, L. Athanasiou, D. I. Fotiadis, L. K. Michalis, and P. W. Serruys, "Hybrid intravascular imaging: current applications and prospective potential in the study of coronary atherosclerosis," J. Am. Coll. Cardiol. **61**(13), 1369–1378 (2013).
2. N. D. Gladkova, E. V Gubarkova, E. G. Sharabrin, V. I. Stelmashok, and A. E. Beimanov, "The potential and limitations of intravascular optical coherence tomography," Sovrem. Tehnol. v Med. **2012**, 128–141 (2012).
3. A. Maehara, G. S. Mintz, and N. J. Weissman, "Advances in intravascular imaging," Circ. Cardiovasc. Interv. **2**(5), 482–490 (2009).
4. J. J. Wentzel, A. G. van der Giessen, S. Garg, C. Schultz, F. Mastik, F. J. H. Gijsen, P. W. Serruys, A. F. W. van der Steen, and E. Regar, "In vivo 3D distribution of lipid-core plaque in human coronary artery as assessed by fusion of near infrared spectroscopy-intravascular ultrasound and multislice computed tomography scan," Circ Cardiovasc Imaging **3**(6), e6–e7 (2010).
5. S. Verheye, G. R. Y. De Meyer, R. Krams, M. M. Kockx, L. C. A. Van Damme, B. Mousavi Gourabi, M. W. M. Knaapen, G. Van Langenhove, and P. W. Serruys, "Intravascular thermography: Immediate functional and morphological vascular findings," Eur. Heart J. **25**(2), 158–165 (2004).
6. J. E. Muller, N. J. Weissman, and E. M. Tuzcu, "The year in intracoronary imaging," JACC Cardiovasc. Imaging **3**(8), 881–891 (2010).
7. S. E. Nissen, J. C. Gurley, C. L. Grines, D. C. Booth, R. McClure, M. Berk, C. Fischer, and A. N. DeMaria, "Intravascular ultrasound assessment of lumen size and wall morphology in normal subjects and patients with coronary artery disease," Circulation **84**(3), 1087–1099 (1991).
8. S. Sethuraman, J. H. Amirian, S. H. Litovsky, R. W. Smalling, and S. Y. Emelianov, "Spectroscopic intravascular photoacoustic imaging to differentiate atherosclerotic plaques," Opt. Express **16**(5), 3362–3367 (2008).
9. B. Wang, J. L. Su, J. Amirian, S. H. Litovsky, R. Smalling, and S. Emelianov, "Detection of lipid in atherosclerotic vessels using ultrasound-guided spectroscopic intravascular photoacoustic imaging," Opt. Express **18**(5), 4889–4897 (2010).
10. B. Wang, A. Karpiouk, D. Yeager, J. Amirian, S. Litovsky, R. Smalling, and S. Emelianov, "In vivo Intravascular Ultrasound-guided Photoacoustic Imaging of Lipid in Plaques Using an Animal Model of

#270504 http://dx.doi.org/10.1364/BOE.7.004441
Journal © 2016 Received 18 Jul 2016; revised 27 Sep 2016; accepted 30 Sep 2016; published 6 Oct 2016

Biomedical Optics EXPRESS

Atherosclerosis," Ultrasound Med. Biol. **38**(12), 2098–2103 (2012).
11. M. Wu, K. Jansen, A. F. W. van der Steen, and G. van Soest, "Specific imaging of atherosclerotic plaque lipids with two-wavelength intravascular photoacoustics," Biomed. Opt. Express **6**(9), 3276–3286 (2015).
12. X. Ji, K. Xiong, S. Yang, and D. Xing, "Intravascular confocal photoacoustic endoscope with dual-element ultrasonic transducer," Opt. Express **23**(7), 9130–9136 (2015).
13. T. J. Allen, A. Hall, A. P. Dhillon, J. S. Owen, and P. C. Beard, "Spectroscopic photoacoustic imaging of lipid-rich plaques in the human aorta in the 740 to 1400 nm wavelength range," J. Biomed. Opt. **17**(6), 061209 (2012).
14. J. Zhang, S. Yang, X. Ji, Q. Zhou, and D. Xing, "Characterization of lipid-rich aortic plaques by intravascular photoacoustic tomography: ex vivo and in vivo validation in a rabbit atherosclerosis model with histologic correlation," J. Am. Coll. Cardiol. **64**(4), 385–390 (2014).
15. K. Jansen, A. F. W. van der Steen, H. M. M. van Beusekom, J. W. Oosterhuis, and G. van Soest, "Intravascular photoacoustic imaging of human coronary atherosclerosis," Opt. Lett. **36**(5), 597–599 (2011).
16. Y. Fan, A. Mandelis, G. Spirou, and I. A. Vitkin, "Development of a laser photothermoacoustic frequency-swept system for subsurface imaging: theory and experiment," J. Acoust. Soc. Am. **116**(6), 3523–3533 (2004).
17. K. Maslov and L. V. Wang, "Photoacoustic imaging of biological tissue with intensity-modulated continuous-wave laser," J. Biomed. Opt. **13**(2), 024006 (2008).
18. S. A. Telenkov and A. Mandelis, "Photothermoacoustic imaging of biological tissues: maximum depth characterization comparison of time and frequency-domain measurements," J. Biomed. Opt. **14**(4), 044025 (2009).
19. S. Telenkov, R. Alwi, A. Mandelis, and A. Worthington, "Frequency-domain photoacoustic phased array probe for biomedical imaging applications," Opt. Lett. **36**(23), 4560–4562 (2011).
20. B. Lashkari and A. Mandelis, "Linear frequency modulation photoacoustic radar: optimal bandwidth and signal-to-noise ratio for frequency-domain imaging of turbid media," J. Acoust. Soc. Am. **130**(3), 1313–1324 (2011).
21. S. Telenkov and A. Mandelis, "Signal-to-noise analysis of biomedical photoacoustic measurements in time and frequency domains," Rev. Sci. Instrum. **81**(12), 124901 (2010).
22. A. B. Karpiouk, B. Wang, and S. Y. Emelianov, "Development of a catheter for combined intravascular ultrasound and photoacoustic imaging," Rev. Sci. Instrum. **81**(1), 014901 (2010).
23. S. A. Telenkov and A. Mandelis, "Fourier-domain biophotoacoustic subsurface depth selective amplitude and phase imaging of turbid phantoms and biological tissue," J. Biomed. Opt. **11**(4), 044006 (2006).
24. G. S. Kino, *Acoustic Waves: Devices, Imaging, and Analog Signal Processing* (Prentice Hall, 1987).

1. Introduction

One of the leading causes of death worldwide is coronary artery disease [1]. To improve the current understanding of the disease, effective in-vivo imaging of atherosclerotic plaque progression is necessary for better management of major cardiac events, occlusive thrombosis and plaque vulnerability. Advances in engineering and the miniaturization of medical devices have allowed numerous intravascular imaging techniques to emerge over the last decade, after it became apparent that contrast coronary angiography has significant limitations – namely, that angiography can only provide two-dimensional projections of the vessel structures without any compositional information of the vessel walls [1]. Intravascular optical coherence tomography (OCT) provides high spatial resolution of plaques, however it produces weak signals from lipids, making it difficult to distinguish it from other low contrast features [2]. It is also limited in penetration depth due to optical scattering, especially in the presence of arterial blood, requiring an optically transparent flush prior to imaging [3]. Other modalities such as Raman or diffuse reflectance near-infrared (NIR) spectroscopy can provide composition information of lipid cores, but do not provide depth resolved structural information [4–6].

Intravascular ultrasound (IVUS) is a commonly used clinical imaging tool and can provide important information on disease development, such as vessel dimensions, plaque progression, vessel remodeling, and identifying calcifications [1,7]. However, it does suffer from limited acoustic contrast between soft tissues and thus cannot characterize plaque composition reliably [1,8]. Alternatively, intravascular photoacoustic (IVPA) imaging has the potential to detect and characterize the presence and composition of atherosclerotic plaques and is currently in active development [9–12]. Its major advantage over most optical imaging methods is that it does not rely solely on ballistic photons; by converting optical contrast into acoustic energy, it is able to image more deeply than its purely optical counterparts. Also, by using multiple excitation wavelengths, one can spectroscopically probe for different information within the tissue of interest [8,11–14]. By combining IVPA imaging and IVUS

Biomedical Optics EXPRESS

into a hybrid imaging modality, it has been shown that it may be possible to enhance the diagnostic capability to differentiate lipids in atherosclerosis in-vivo [8,15].

Almost universally, IVPA imaging has been demonstrated using the pulsed photoacoustic (PA) technique whereby a short nanosecond pulsed laser is used to generate the PA waves. Such lasers are relatively large in size (electronics and cooling unit), can exhibit instability between pulses, lack robustness (needing regular alignment and maintenance), and are expensive. Another PA method to image biomedical tissue using an intensity-modulated continuous wave (CW) laser is called Frequency Domain Photoacoustics (FDPA) [16,17]. It has been shown that this technique can be used for spatially-resolved PA imaging with a single element detector and phased sensor arrays [18,19]. The method uses intensity-modulated optical pulses emitted by a CW laser that codes the PA signal and provides signal compression, similar to radar. By using this approach, the mean power of the CW laser beam can be much lower than the peak powers employed in pulsed PA techniques, allowing the use of smaller laser systems. Because of the lower power requirements, CW diode lasers become an attractive option as they are inexpensive, portable, robust, and stable when compared to a Q-switched design. Additionally, they do not need to be actively cooled, especially at lower output powers. However, since the amplitude of these CW PA waves are lower when compared to pulsed PA, signal processing methods such as matched filtering, need to be employed to detect the coded PA response within the noise [20,21].

This paper aims to demonstrate a novel method of IVPA imaging using frequency domain photoacoustics, denoted FD-IVPA. We show the feasibility of using this technique with a CW laser and a dual-imaging platform capable of IVUS and FD-IVPA imaging. A transducer probe was designed and both imaging techniques are demonstrated on an agar vessel phantom with embedded targets using the same probe. This study, to the knowledge of the authors, is the first such demonstration of FDPA for potential intravascular applications.

2. Materials and methods

2.1 Imaging assembly

The imaging assembly consisted of two parts: an optical fiber and acoustic transducer. For ease of construction and alignment, a side-firing fiber design was used [22]. The optical fiber (FiberOptics Systems Inc., Simi Valley, CA, USA) consisted of a 600µm multimodal fiber that was polished at an angle of 33° and placed inside a quartz tube (Sutter Instruments Co., Novato, CA, USA). This ensured the tip was coupled with air, thus reflecting the light outwards in the desired direction, allowing co-alignment with the acoustic beam.

The ultrasound transducer was designed and built in-house. PiezoCAD (Sonic Concepts Inc., Bothell, Washington, USA) was used to determine the materials and dimensions. The active element was made of PZT 3203HD (CTS Corp., Albuquerque, New Mexico, USA) with dimensions of 2mm by 2mm chosen to minimize the electrical input impedance. A 7MRayl matching layer of tungsten powder-loaded Epotek H20E epoxy (Epoxy Technology Inc., Billerica, Massachusetts, USA) was added to the transducer face to improve the sensitivity and bandwidth. Based on the simulations, the thicknesses of the PZT and matching layer were chosen to be 250µm and 60µm, respectively. H20E epoxy was used to create a 1mm-thick backing layer and both signal and ground connections to a micro-coaxial cable. The centre frequency and −6dB bandwidth of the transducer was measured in pulse-echo mode and found to be 8.5MHz and 100%, respectively.

The transducer was mounted on the side of a hollow brass rod with an outer diameter of 2.5mm. The optical fiber was placed within the quartz tube allowing axial and rotational movement. This allowed flexibility during co-alignment to attain maximum FDPA signal. To allow the light to exit, a slit was cut into one end of the rod that ran longitudinally for approximately 3mm. The fiber was then aligned such that the light was directed through the slit in the brass rod and co-aligned with the transducer as shown in Fig. 1(a). The entire

Biomedical Optics EXPRESS

optical assembly was then locked in place within the brass rod prior to imaging. A photograph of the assembled probe is shown in Fig. 1(b).

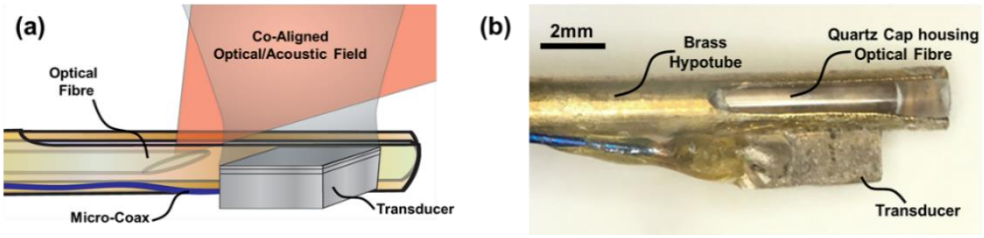

Fig. 1. (a) Probe design at the distal end of the imaging probe; (b) Image of the IVUS/FD-IVPA probe mounted on a brass rod.

2.2 Experimental setup

The setup was designed such that the IVUS/FD-IVPA imaging assembly stayed stationary while the target to be imaged rotated around its axis. A motorized rotary stage holding the phantom was placed inside a water tank and centered with respect to the static transducer assembly. A schematic of the experimental setup is shown in Fig. 2. A cylindrical vessel phantom with lumen of 6mm in diameter was made of 2% agar. The vessel phantom was placed upright on the rotary stage and imaging assembly was lowered within its lumen. The laser (OmniPulse Technology Corp., HFDD-12-1-25M, San Diego, CA, USA) with a mean power of 1W at 1210nm was used to generate PA response. Using the rotary stage, photoacoustic and ultrasound signals were recorded with increments of 1°. Two phantoms each containing different targets were imaged in the experiments. The first phantom consisted of two graphite rods, with a diameter of 0.8mm that were place within the agar vessel phantom. The second phantom had two wall-less channels measuring 1.5mm in diameter in which butter was embedded to mimic atherosclerotic lipid deposits.

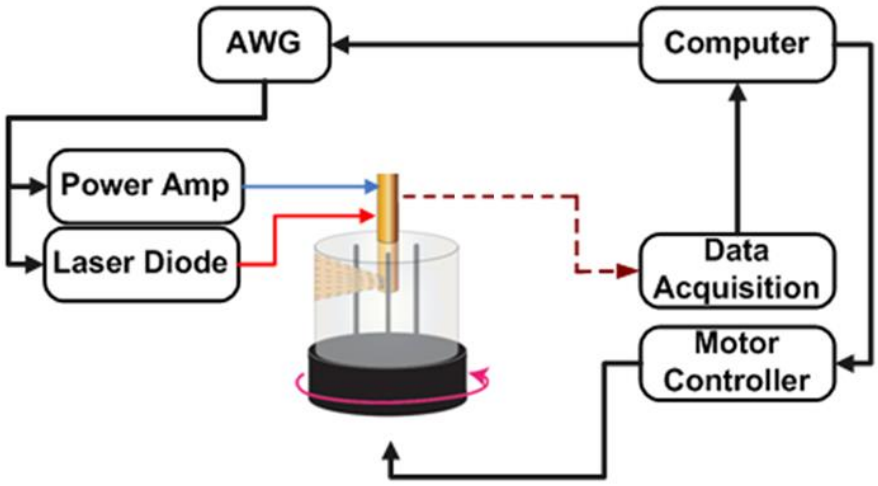

Fig. 2. Schematic of experimental setup.

2.3 Data acquisition and image processing

At each azimuthal position of the rotating stage, two A-lines were acquired by the same transducer: standard IVUS (pulse/echo) and FD-IVPA signals. A $20V_{pp}$ Gaussian modulated 8.5MHz single cycle was used to acquire the IVUS data. The signals were averaged 8 times and captured using an oscilloscope (MSO4032, Tektronix Inc., Beaverton OR, USA). Following acquisition of the ultrasound data, the same target area was exposed to the

Biomedical Optics EXPRESS

modulated laser beam to record the photoacoustic signal. The laser diode was modulated using linear chirp waveforms of 0.5ms in duration with a 50% duty cycle.

The chirp-modulated laser beam generates a train of photoacoustic signals with the same temporal characteristics as the optical chirps. The received acoustic pressure signals at each azimuthal position were digitized with the same oscilloscope and stored for subsequent processing. Since the energy of a single laser chirp was relatively low (~1mJ), the generated photoacoustic response is comparatively weak as compared to the pulsed photoacoustic technique. To increase signal-to-noise ratio (SNR) of the PA measurements, eight acoustic pressure signals were coherently averaged. This averaged data, p(t), was cross-correlated with a reference chirp, *r(t)*, see Fig. 3(a), using a Fourier domain implementation to compress the energy of the received signals [23]. The entire processing algorithm was implemented in the frequency domain using fast Fourier transforms (FFT) applied to the received signals, *p(t)*, and the modulation waveform, *r(t)*. Since the Fourier spectrum of the modulation chirps is bandlimited by the receiving transducer (4MHz-12MHz), as shown in Fig. 3(b), the noise power can be reduced using a bandpass filter tuned to the chirp bandwidth. The time domain cross correlation signal, *s(t)*, is computed in Matlab using the following equation:

$$s(t) = \mathcal{F}^{-1}\left\{W(\omega) * R^{*}(\omega) * P(\omega)\right\}. \tag{1}$$

where $P(\omega)$, $R(\omega)$ represent the Fourier spectra of the transducer signal and the modulation waveform respectively, and $W(\omega)$ is the spectral weighting function used to limit the bandwidth and reduce the sidelobe level. The correlation processing algorithm employed for detection of photoacoustic signals provides significant increase of SNR by compressing the entire signal energy into a short correlation peak [23]. Assuming that incoming signals with amplitude A_0 are accompanied by white noise with the power spectral density $N_0/2$, the matched filter output SNR is given by:

$$SNR_{out} \sim \frac{E}{N_o}. \tag{2}$$

where $E \sim A_o^2 T_{ch}$ is the signal energy and T_{ch} is the chirp duration [24]. Since the input SNR is estimated as:

$$SNR_{in} \sim \frac{A_o^2}{N_o \Delta f}. \tag{3}$$

where Δf is the chirp bandwidth, overall SNR gain due to matched filter processing is:

$$\frac{SNR_{out}}{SNR_{in}} \sim T_{ch}\Delta f. \tag{4}$$

Thus, use of linear chirped signals with high time-bandwidth product can potentially provide an increase in SNR by ~20dB–40dB [21]. An example of the correlation processing of a noisy signal with the input SNR = –30dB and 8 averages is shown in Fig. 3(c). The application of matched filter compression in the context of photoacoustic measurements enables the use of relatively low power CW laser diodes for imaging applications. The resulting cross-correlation signal, *s(t)*, in the time domain, is combined with the acquired acoustic A-line. From this, the position of the acoustic sources within the phantom are identified by the correlation peak delay times – while the width of correlation signal defines the axial resolution which is a function of the chirp bandwidth [18]. Although the theoretical resolution limit for a 4–12MHz chirp is approximately 180µm, the spectral window $W(\omega)$ broadens the correlation peak to ~285µm FWHM while simultaneously reducing the side lobes to the –42dB level.

Biomedical Optics EXPRESS

Finally, the IVUS and FD-IVPA images were reconstructed separately by taking each A-line, *s(t)*, and generating radial images by scan converting them into the Cartesian coordinate system using a cubic interpolation method. To demonstrate that the images were inherently co-registered, a composite image was created by overlaying the FD-IVPA image onto the IVUS image.

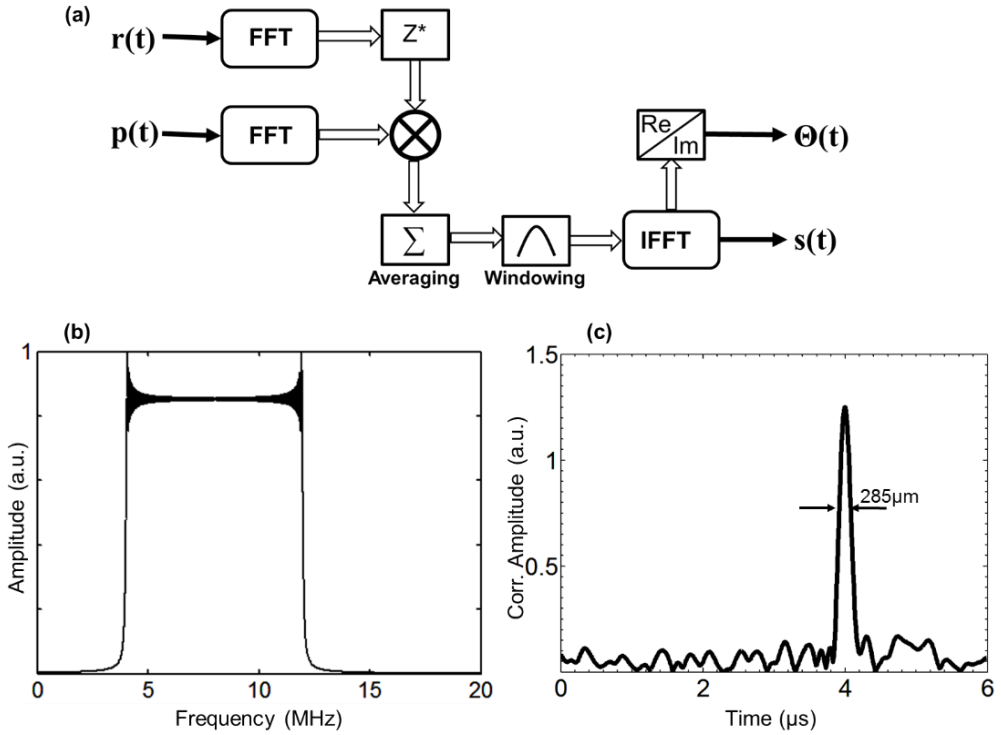

Fig. 3. a) Block-diagram of FD correlation processing; b) Fourier spectrum of laser modulation; c) Computed correlation signal for input SNR = –30dB and 8 averages.

3. Results

Using the above experimental setup, IVUS and FD-IVPA A-lines were acquired separately, at each azimuthal position of the rotational stage, using the same imaging probe. This first demonstration was on graphite targets located at eleven o'clock and four o'clock within the phantom. The reconstructed FD-IVPA image, the IVUS image using traditional pulse/echo and a composite of the two images are shown in Fig. 4(a-c). The dynamic range of the FD-IVPA and IVUS images with graphite targets are 21dB and 55dB, respectively. Next, an agar phantom containing butter targets were imaged to demonstrate the ability of FD-IVPA to image lipids. The targets were placed within the agar phantom at one o'clock and eight o'clock. The images are shown in Fig. 4(d-f). As seen in Fig. 4(d) the targets are clearly visible as there is strong PA image contrast. The two locations where butter was placed within the phantom can be clearly detected using this method. The dynamic range of the FD-IVPA and IVUS images in Fig. 4(d and e) are 16dB and 37dB, respectively. No image registration has been performed in displaying the composite images in Fig. 4(c and f). Travel time information between the one way (PA) signal versus two way (IVUS) travel was accounted for during reconstruction.

Biomedical Optics EXPRESS

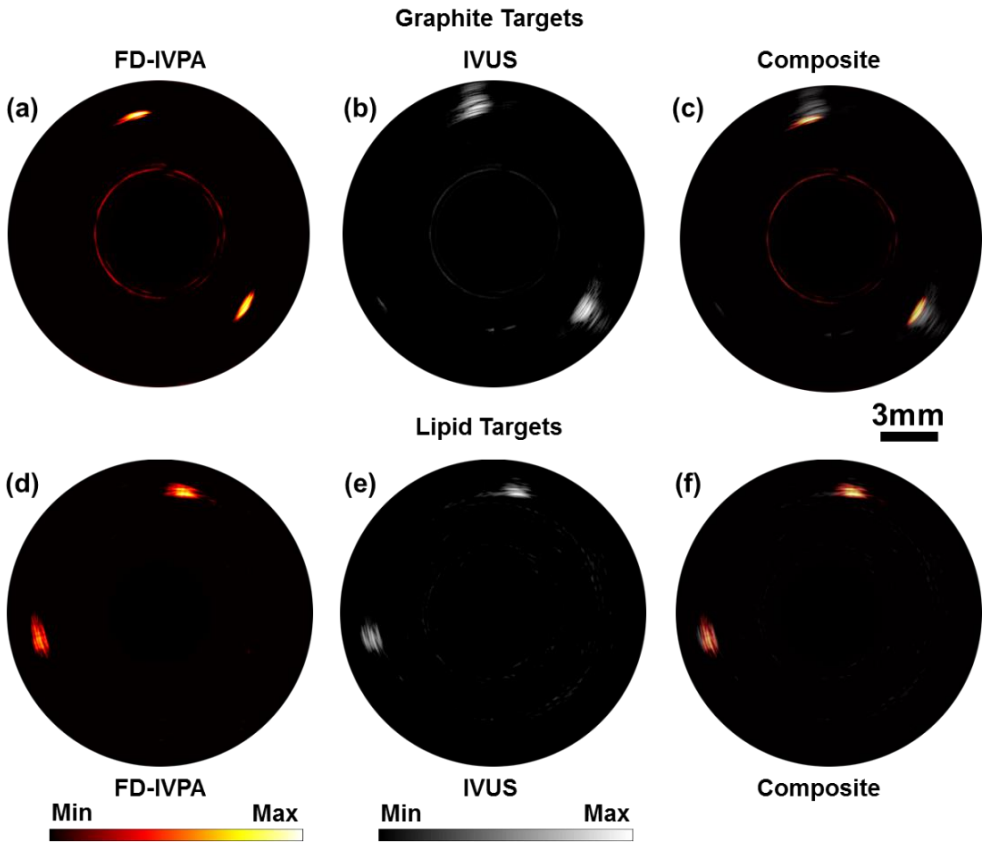

Fig. 4. (a-c) Images of a vessel phantom with graphite targets and (d-f) Images of a vessel phantom with lipid targets. FD-IVPA imaged at 1210nm.

4. Discussion

The paper demonstrates the feasibility of using FD-IVPA as an imaging modality for intravascular applications. This is demonstrated using graphite and butter targets in agar vessel phantoms and imaged at 1210nm. Although we validated the technique using an 8.5MHz transducer, which is lower in frequency (and resolution) than clinical IVUS devices, it is not an inherent constraint of FD-IVPA. It is common to find CW laser diodes with response times that are much shorter than the modulation rates needed for clinically relevant frequencies, so practically, the optical coding can be done at much higher rates and thus, not a limiting factor.

Modifications are needed to make an IVUS probe FD-IVPA capable. Due to the common imaging probe used for detection in both modalities, an optical fibre co-aligned with the field of view of the IVUS transducer is the only additional requirement and, unlike other optical techniques that depend on ballistic photons, minimal consideration to light scattering within the tissue is needed. The construction of the acoustic probe for FD-IVPA applications and the light delivery mechanism do not differ in the fundamental concepts from pulsed IVPA probe designs. Thus, although the acoustic probe used in this study is large, the physical footprint can be reduced to clinically relevant dimensions depending on the imaging application. Furthermore, sophisticated software registration is not needed since the images attained are innately co-registered, as shown in Fig. 4(c and f).

As in pulsed IVPA imaging, FD-IVPA is sensitive to optical contrast. Therefore, spectroscopic techniques can be used to potentially differentiate distribution, type and size of

Biomedical Optics EXPRESS

lipid or collagen formations inside a vessel. By switching between multiple wavelengths one could assess the characteristics of certain tissues by the PA response generated due to preferential absorption. When using pulsed techniques, switching between wavelengths can be slow, such as when mechanical switching is employed in an optical parametric oscillator design, or grossly expensive if multiple pulsed lasers are used. Since CW diodes are relatively inexpensive, multiple diode packages can be used and driven by the same (or multiple) laser driver(s). Electronic switching can be extremely fast, cost sensitive, easier to implement and can be a significant advantage to this imaging modality.

The chirp duration used in the experiments above was selected to balance SNR with exposure time per A-line. With longer chirp durations, greater SNR can be achieved; however, if one is considering reducing the chirp length while retaining the same SNR, more average optical power needs to be delivered to the target. Two options can be employed: i) use a higher output CW diode laser or ii) drive several lower power diodes simultaneously. To get more average optical power using a larger CW diode, one needs to drive current into the diode at higher amplitudes. There may be physical limitations to this option if the modulations needed are extremely fast, due to the inherent inductances of the diode package or the driver, limiting how fast this can be performed practically. Alternatively, it is much simpler to drive lower currents into a diode at faster modulation frequencies. Thus, employing smaller diodes and driving them in parallel may be an easier approach while gaining the same average optical output. The outputs of the diodes can be coupled into one fibre, providing a gain proportional to the number of diodes used. Care must be taken to ensure the phase delays of the multiple diodes are synchronized for a clean optical signal. Single driver or multiple driver configurations can be chosen depending on power requirements and application constraints. Another consideration when choosing the chirp duration is temporal resolution. In this study we use a 0.5ms on/off chirp scheme, with a 50% duty cycle, which is significantly slower than what is required for clinical applications. SNR can be maintained by increasing the optical power delivered to the tissue and reducing the chirp length as discussed above. Practically, however, one cannot increase the optical power output indefinitely, as it is limited by ANSI safety standards, but a significant reduction in the time of the modulation scheme can be achieved using this method. Alternatively, a multi-element detector approach may be most promising in achieving clinical imaging speeds, eliminating the need for rotation completely and allowing one image frame per optical chirp.

A drawback of using discrete CW laser diodes is the limitation of wavelengths that are commercially and readily available. This can make it difficult to employ this technique if a particular wavelength needed is not available. Fortunately, high power diodes are available at wavelengths such as 1210nm and 1720nm which represent relative peaks in lipid optical absorption [11,13]. Also, many other wavelengths are widely available for spectroscopic imaging applications. Care must be taken in the development of the laser diode drivers with multiple wavelengths since these diodes have inherent variations in the inductances of their packages, different conversion efficiencies and different electrical specifications which can make the output power and maximum modulation frequencies between diodes vary considerably, if one is not careful.

5. Conclusion

The paper shows the feasibility of using FD-IVPA as a novel imaging modality for intravascular applications. This was achieved using a CW laser and coding the excitation sequences using an intensity modulation scheme. The results show that FD-IVPA gives complementary information to IVUS with inherent registration due to the use of a common detector with minimal modifications. Since PA imaging, and thus FD-IVPA, is sensitive to optical contrast, spectroscopic imaging using multiple wavelengths can be potentially used to image and characterize lipid and collagen formations within the vessel.

Biomedical Optics EXPRESS

Funding

Natural Sciences and Engineering Research Council of Canada (NSERC); Canadian Institutes of Health Research (CIHR).